Nanoscale Advances

REVIEW

View Article Online
View Journal | View Issue

Cite this: *Nanoscale Adv.*, 2024, **6**, 3476

Analytical developments in the synergism of copper particles and cysteine: a review

Priyanka Sharma,[a] Mainak Ganguly *[a] and Ankita Doi[b]

Cysteine, a sulfur-containing amino acid, is a vital candidate for physiology. Coinage metal particles (both clusters and nanoparticles) are highly interesting for their spectacular plasmonic properties. In this case, copper is the most important candidate for its cost-effectiveness and abundance. However, rapid oxidation destroys the stability of copper particles, warranting the necessity of suitable capping agents and experimental conditions. Cysteine can efficiently carry out such a role. On the contrary, cysteine sensing is a vital step for biomedical science. This review article is based on a comparative account of copper particles with cysteine passivation and copper particles for cysteine sensing. For the deep understanding of readers, we discuss nanoparticles and nanoclusters, properties of cysteine, and importance of capping agents, along with various synthetic protocols and applications (sensing and bioimaging) of cysteine-capped copper particles (cysteine-capped copper nanoparticles and cysteine-capped copper nanoclusters). We also include copper nanoparticles and copper nanoclusters for cysteine sensing. As copper is a plasmonic material, fluorometric and colorimetric methods are mostly used for sensing. Real sample analysis for both copper particles with cysteine and copper particles for cysteine sensing are also incorporated in this review to demonstrate their practical applications. Both cysteine-capped copper particles and copper particles for cysteine sensing are the main essence of this review. The aspect of the synergism of copper and cysteine (unlike other amino acids) is quite promising for future researchers.

Received 17th April 2024
Accepted 15th May 2024

DOI: 10.1039/d4na00321g

rsc.li/nanoscale-advances

1. Motivation

Capping agents play a pivotal role in the synthesis of copper particles. In colloidal synthesis, capping compounds play a crucial role as stabilizers that limit the growth of nanoclusters (NACs) and stop them from aggregating or coagulating. The ligands used as capping agents maintain the stability of the

[a]*Department of Chemistry, Manipal University Jaipur, Dehmi Kalan, Jaipur 303007, India. E-mail: humansense2009@gmail.com*

[b]*Department of Biosciences, Manipal University Jaipur, Dehmi Kalan, Jaipur 303007, India*

Priyanka Sharma

Priyanka Sharma obtained her BSc and MSc degrees from Maharaja Brij University in India. She is now pursuing her PhD degree at Manipal University Jaipur, India, under the guidance of Dr Mainak Ganguly. Her areas of interest are material science and environmental science.

Mainak Ganguly

Dr Mainak Ganguly received his PhD degree from the Indian Institute of Technology, Kharagpur, India in 2014. He had acted as postdoctoral researcher up to 2019 at Furman University (USA) and McGill University (Canada). He is currently working as an asst. professor in the Department of Chemistry, Manipal University Jaipur (India). His research interests include nanoparticles, clusters, biophysical chemistry, and environmental remediations. He has published more than 60 papers and two book chapters.

interface between the nanoparticles (NAPs) and the preparation medium.[1–3] The surface composition and size distribution of these NAPs change if they are coated with capping agents.[4,5] By halting their non-specific interaction, NAPs are more compact, which reduces aggregation and improves their biocompatibility and non-toxicity.[6]

Cysteine is a very important biological molecule. The capping of NAPs and NACs with cysteine is an active area of research. On the other hand, copper nanoparticles (CuNAPs) and nanoclusters (CuNACs) are gaining increasing importance due to their inexpensiveness and abundance in nature. However, their rapid aerial oxidation limits their practical applications. In this regard, cysteine is employed by many research groups for the synthesis and stability of copper particles. However, to the best of our knowledge, cysteine-passivated coinage particles, highly promising for the present generation, have not at all been reviewed in any form.

In this review, we address all such lacunas in detail to enrich the literature for upcoming researchers. A comparative account has been drawn here for the first time regarding copper particles with cysteine capping and comprehensive cysteine sensing with copper particles. Moreover, the synergism of copper and cysteine is pivotal in this area. As mentioned, to the best of our knowledge, no review containing such synergism has yet been published.

2. Introduction

NAPs are omnipresent[1] and can be synthesized naturally. When NAPs are less than 2 nm in size, they are called nanoclusters (NACs).[2] A great effort has been paid to the synthesis of both NACs and NAPs in the laboratory for versatile applications. The stability and tuning of the size and morphology are a challenge in the current research. In this context, the choice of capping agents and experimental conditions are crucial [Fig. 1]. NAPs are particles with at least one dimension in the 1–99 nm range.[3] The surface plasmon band of nanoparticles refers to the collective oscillation of electrons on the nanoparticle surface,[4] resulting in a characteristic absorption peak in the UV-visible spectrum, crucial for applications in sensing, imaging, and catalysis.[5] Over the past ten years, interest in NACs —near monodispersed particles typically smaller than 10 nm (100 Å) in diameter — has increased significantly.[6,7] However, some scientists also consider NAPs sized < 2 nm as nanoclusters.[8] Surface plasmon bands are lost in NACs with their discrete energy levels, responsible for emissive properties. NACs are rightly considered to be the missing link between atoms and NAPs.[9]

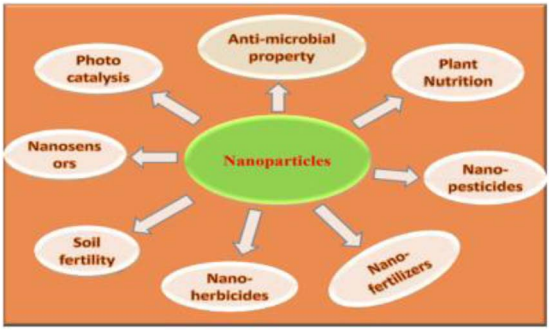

Fig. 1 Illustration of the general applications of nanoparticles.

Capping agents are organic compounds that bind to the surface of NAPs, and are often utilized in the synthesis of small-sized NAPs to regulate their growth and agglomeration.[10–13] To effectively function in the living system, capping agents should be biodegradable, widely distributed and soluble, biocompatible, and non-toxic.[14] The steric barrier caused by the covalent interaction between the chains of capping ligands and the surface of the NAPs gives the nanocomposite its ultimate stability. At the nanoscale, there are more atoms on the surface, and capping boosts this number even more.[15] Additionally, suitable capping agents reduce NAPs aggregation for a longer period. The capping agent is often an amphiphilic molecule with a non-polar hydrocarbon tail and a polar head group.[10,16] Capping agents confer functionality and improve compatibility with another phase, because of their amphiphilic phase. Various capping agents, such as surfactants, tiny ligands, polymers, dendrimers, cyclodextrins, and polysaccharides, have been utilized in the formation of NAPs and NACs. These have all been used as capping agents with great success because they can cause minor modifications in nanomaterials that have powerful medicinal and environmental cleansing effects.[17,18] Sometimes the capping agent acts as both a reducing and stabilizing agent. For example, salicylaldehyde is both a reducing agent and a stabilizing agent that can be used for the formation of coinage metal particles.[19,20]

A nanomaterial, a detection element that gives specificity, and a sign transduction system that provides a way of reporting the existence of an analyte are the three elements that make up nanomaterial-enabled sensors. Though each nanosensor can be classified using these three categories, these parts are not always different entities within a sensor.[21] Multiplex detection, which refers to the ability of a sensor to detect numerous analytes, is also possible. Some sensors depend on a "turn-off" or "on/off" mechanism, which detects analytes by producing a signal as well as turning them on or off when there is a decline in a signal[22] [Fig. 2].

Ankita Doi

Ankita Doi graduated from Alankar P. G. Mahavidyalaya (Jaipur, Rajasthan, India), followed by postgraduate study at Alankar P. G. Mahavidyalya (Jaipur, Rajasthan). Currently, she is pursuing a PhD at Manipal University, Jaipur, under the supervision of Dr Mainak Ganguly. Her key research area is nanoparticles.

Amino acids (AAs) are the primary building blocks of the metabolism and serve as precursors to a variety of neurotransmitters and hormones. Proteins are the primary building blocks of several metabolites, including primary, secondary, and nucleic acids. They are necessary for cellular metabolism and nourishment.[23] The inclusion of both carboxylic acid and amine functional groups in the chemical structure of all AAs is a common trait. Moreover, amino acids are often used as a capping agent for forming nanomaterials.[24] Such amino acid-capped nanomaterials are widely used in biological and chemical applications. On the other hand, much research has been done for amino acid sensing, as amino acids are important biological molecules. AuNACs as sensing platforms for phenylalanine in the presence of comparative molecules were investigated by Sadeghan *et al.* with a study on iodide.[25] While N_2-doped graphene quantum dots were investigated by Dhrishya *et al.*,[26] who demonstrated the potential of ultrastable gold–copper NACs for the selective electrochemical and luminescent detection of glycine. To sense temperature and detect arginine, Wang *et al.*[27] demonstrated the supramolecular self-assembly of atomically precise AgNACs with chiral peptides. Cysteine (cyst) is one of the most important amino acids due to its potential in diverse *in vivo* and *in vitro* applications. Cysteine-capped silver nanoparticles (Ag NAPsCyst) for the sensitive and specific colorimetrical sensing of vitamin B1 in food and aquatic samples were demonstrated by Khalkho *et al.*[28] The selective sensing of cysteine/AgNAPs cyst was also demonstrated by Athilakshmi *et al.*[29]

One of four metals—gold, silver, bronze, or copper—was used to make most ancient and medieval coins. Coinage metals have fascinating plasmonic properties and so have sparked a lot of research. In addition, coinage metal clusters have adjustable fluorescence. Copper is the most significant contender in this category because of its availability and affordability.[22]

In this review article, we present a comparative account of cysteine with copper nanoparticles and nanoclusters for the first time. Cysteine-capped copper particles (both clusters and nanoparticles) are reviewed together with their applications. On the other hand, the employment of copper particles for cysteine sensing is also covered in detail. Thus, copper particles with cysteine and for cysteine sensing are the main focus of the present review article.

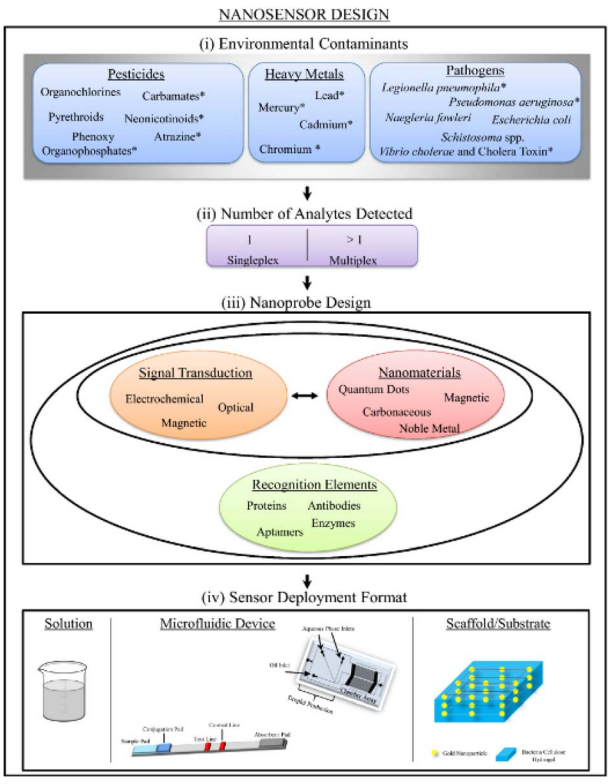

Fig. 2 Schematic representation for the design of nanosensors for environmental contaminants, also indicating the number of analytes detected, nanoprobe design, and a sensor deployment format.[22]

3. Choice of copper in nanoscience

Due to global research and development, nanotechnology—one of the key scientific revolutions of the twenty-first century—has swiftly advanced. The production of matter at the nanoscale is of primary importance for the development of this subject.[30] NAPs are particles with at least one dimension and a maximum size of 100 nm.[31] Quantum dots may not have any dimensions in this situation. Due to quantum effects and their high surface-to-volume ratio, metal NAPs exhibit remarkable UV-visible sensitivity and electrical, catalytic, thermal, and antibacterial capabilities.[32,33] Zero-valent copper (Cu^0), which is most stable as solid, spheroidal structures with diameters between 10–50 nm, often takes the form of reduced copper ions bonded together in an organized lattice structure. A broad double-peaked plasmon resonance was observed in copper nanoshells, where the plasmon resonance (dipole or quadrupole) of the copper nanoshell overlapped with the interband transitions of copper. The dipolar plasmon resonance was found to rely on the shape of the copper nanocrystals (a few nm in size), specifically triangular prisms, elongated particles, cylinders, and spheres. In contrast to Ag and Au, Cu metal may not be the best plasmonic material due to the heterogeneity in the size and shape of the samples and the lack of control over the interparticle distances, which can lead to widened surface plasmon resonances. CuNAPs have a deep red color because they absorb a lot of light in the violet-to-orange spectrum (400–610 nm) but are transparent to red light (light with a wavelength greater than or equal to 635 nm). Surface plasmon resonance (SPR), which corresponds to the band of green-yellow light at 570 nm, is the result of the collective fluctuation of the outward valence electrons (4s for Cu) brought on by a resonant interaction with the oscillating electric field of incident light.[4]

Moreover, Cu particles are applied in many different domains, including chemical production, biological applications, energy conversion and storage, and environmental technologies. The various synthetic methods for developing Cu and Cu-based nanoparticles (metallic copper, copper oxides, and hybrid copper nanostructures), as well as copper nanoparticles supported or immobilized on different types of support

materials (SiO_2, magnetic support materials, *etc.*) and their uses in catalysis, were reviewed by Gawande *et al.*[34] Lin *et al.*'s[35] review included a comprehensive assessment of copper nanoclusters for water quality monitoring. Xue *et al.*[36] reviewed the synthesis of copper nanoclusters and their use in pollutant analysis [Fig. 3].

In comparison to other precious metals, copper is comparatively abundant and inexpensive. CuNACs, on the other hand, are less stable because of their high oxidation susceptibility, and their luminescence quantum yield is lower. More, molecular-similar and size-reliant ocular and fluorescence features, inherent magnetism, strong chiral responses, and other characteristics comparable to electrons at the Fermi wavelength are all present in metal nanoclusters smaller than 2 nm.[37] In the ultrasmall size regime, which separates the continuum of energy bands into distinct energy strata, the communal fluctuations of conduction band electrons that are typical for plasmonic atoms upon interacting with an electromagnetic field are no longer dominant.[38] Rich molecular-like characteristics are present in the optical absorption spectra of discrete and quantized states. Noble metal clusters have these characteristics in addition to being extremely stable NACs. The stability of atomically accurate CuNACs, however, is a key concern because of the metal's great vulnerability to oxidation.[39,40] Over the past few decades, the stability issue has been substantially resolved by developing synthetic methods, employing mild and inert conditions, and by choosing suitable ligands with distinctive structures and high metal binding affinities.[41]

4. Cysteine

Thiolated amino acids (AAs) are important biological building blocks because they play a vital role in the assembly and structure of proteins. One of the 20 amino acids, L-cyst is a non-essential AA that is crucial for the functioning of the human body.[42] Cyst, for instance, contributes to the stabilization of protein structure. Nevertheless, aberrant [cyst] may be linked to various symptoms, including liver harm, hair depigmentation, and growth retardation.[43–45] Cyst serves as a biomarker for various viruses, including cancer, HIV, and sepsis.[46] Apart from being a biomarker for human viruses, cyst has also been employed in the cosmetic,[47] pharmaceutical,[48] and food industries.[49] The majority of the cysteine used in the baking sector is extracted from human hair and feathers from birds, including goose, ducks, sheep, and pigs.[50,51] Cyst, synthesized through fermentation and enzymatic reaction, has recently been made available by several companies. Nonetheless, these sources only make up a small part of cyst sources worldwide. Cyst is the rate-limiting AA in the intracellular synthesis of glutathione.[52] There is minimal evidence connecting circulating cysteine levels to the incidence of breast cancer, despite the biological plausibility that cyst can have a preventive effect on carcinogenesis.[53]

The cyst biosynthetic route first requires fixing the inorganic sulfur, which is a necessary nutrient for plant growth.[54] Due to the sulfhydryl group's high reactivity, cyst is essential for many biological processes, including delivering the disulfide needed for the intra-molecular cross-connecting of proteins to sustain their double-structures and functions.[55] Additionally, cyst promotes intracellular signal transmission, xenobiotic metabolism, redox activity, and gene regulation. A few disorders have a strong correlation with abnormal cyst levels.[56] Cyst deficiency, for instance, plays a role in disorders such as slower growth.[57–60] The measurement of cyst is significant and has garnered a lot of attention recently. L-Cysteine ($C_3H_7NO_2S$) is an environmentally friendly, cheap, and water-soluble amino acid that is essential for many medicinal goods. It is also a constituent of peptide proteins. It has different functional groups in it, such as sulfur, carboxylic acid, and amines. These functional groups enable this molecule to attach to the surface atoms of different metals with ease. The strongest and most stable binding to metal nanoparticles occurs from their SH group, which permits steady particle dispersion in both aqueous and nonaqueous conditions. Because of this property, L-cysteine serves as a crucial capping molecule during the production of PANs.[61] Not only is cysteine important in protein science but also in nanoscience.[62] Cysteine is water-soluble and may attach to nanoparticle surfaces through a thiolate bond. Furthermore, the surface layer of covalently bonded cysteine molecules can cross-link nanoparticles by hydrogen bond formation. Cysteine-capped nanoparticles are stabilized in an aqueous media by charging the carboxylic acid groups of the cysteine molecules that are attached to their surfaces.[63]

The naturally originated form of cysteine is L-cysteine (L-cyst). Most of the nanoscience research involves L-cyst. Martinez-Comona *et al.*[64] showed the effect of cyst-functionalized

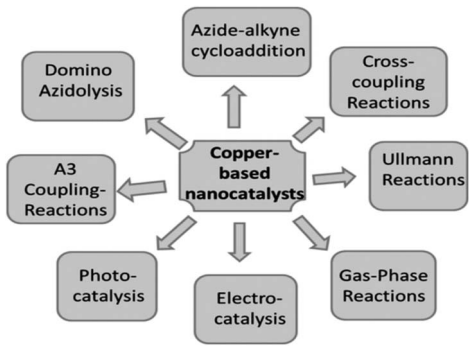

Fig. 3 Use of Cu-based nanocatalysts in various types of reactions.[34]

Fig. 4 Enantioselectivity of cysteine-passivated mesoporous Si nanomaterials.[64]

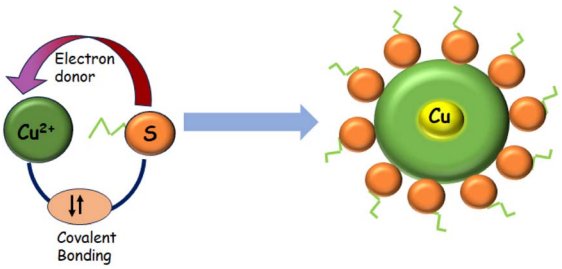

Fig. 5 Mechanism of copper particle formation with cysteine capping.

mesoporous silica NAPs in the context of enantiomers [Fig. 4]. They showed that the chirality significantly influenced the behavior of U87 tumor cells, with D-cyst MSN exhibiting increased internalization and toxicity. Conversely, L-cyst exhibited increased internalization and toxicity in GM08680 healthy cells, indicating that D-cyst MSN might be a useful and targeted therapy for neuroblastoma. After 2 h of incubation, the viability of the bacterial population seemed to be reduced more when L-cyst MSN was used against *S. aureus*, due to its apparently stronger antibiotic properties.

Cyst is also used as a reducing and stabilizing agent for the synthesis of NAPs [Fig. 5]. Though different nanoparticles have been capped *via* cysteine, we focused on copper nanoparticles because of their surface plasmon band in the visible region, high abundance, and cost-effectiveness. Besides, copper nanoclusters are also an active area of research with strong fluorescence properties. Cysteine-capped copper particles have been mostly used in sensing platforms.[65,66] Cyst has been detected using a diversity of analytical methods, including HPLC,[67–69] capillary electrophoresis (CE),[70] electrochemical test,[71,72] UV/vis spectroscopy,[73,74] mass spectrometry,[75] and colorimetric approaches.[76–79]

5. Synergism effect of copper and cysteine

The synergistic effect is the combined effect of two or more species whereby the combined effect exceeds the sum of their separate effects. Synergism is a well-known term in the realm of catalysis. Metals such as Ag, Cu, Ni, Pd, and Co significantly influence oxygen activation in gold-catalyzed oxidation processes. Unlike the other elements in the periodic table, copper and silver, which are in the same group (11), frequently exhibit a synergistic effect.[80] Ganguly *et al.*[81] showed the synergism behavior of gold and silver. Here, we focus on the synergetic behavior of copper and cysteine. The strong interaction between cysteine and copper facilitates the synergistic behavior.

A detailed study was made by Dokken *et al.*[82] regarding copper–cysteine complexes. Cu(II)–cyst complexes were produced with copper(II) sulfate and L-cysteine hydrochloride anhydrous. Cu(II) : cyst complexes were produced in 1 : 2, 1 : 4, and 1 : 6 mole ratios at normal temperatures. First, L-cyst was dissolved in ethanol, followed by copper(II) sulfate. The mixes were then swirled on a heated plate at low temperature. After 0 min, a faint pink precipitate appeared. After the precipitate developed, it was taken off the hot plate. The pale pink precipitate was recovered using vacuum filtration and dried overnight. The precipitate included Cu(II)–cyst complexes.

X-Ray absorption near edge structure (XANES) analysis confirmed that copper remained in the copper(II) state across all the cyst complexes, with similar atomic geometries.[83] Extended X-ray absorption fine structure (EXAFS) data showed that these complexes formed ring structures, with cyst sulfur as the bridging ligands. X-Ray diffraction revealed monoclinic cells in the copper(II)–cyst complexes, with the 1 : 4 copper(II) : cyst complex exhibiting the highest crystallinity. When copper(II) interacted with 2 mole equivalents of cysteine, three sulfur atoms coordinated in the first shell at roughly 2.28 Å, suggesting the presence of copper(II). The suggested structure of the 1 : 2 Cu(II) : cyst complex showed that the sulfur ligands operated as bridging ligands, as evidenced by a copper–copper contact at 2.61 Å. Copper–copper interactions in proteins and other molecules range from 2.56 to 2.70 Å due to bridging with oxygen or sulfur ligands.[84,85] The length of these contacts was significantly less than that of crystals in which the copper is not bridged by another ligand. Between two and three sulfur ligands, copper and sulfur were positioned at a spacing between them of around 2.27 Å. The complex exhibited a higher number of copper–copper links, as evidenced by the copper–copper interaction increasing to around three copper atoms at an interatomic distance of 2.62 Å [Fig. 6].

When Cu^{2+} was added to a cyst solution (pH 7.4), the absorbance peaks were recorded at 260 nm and 300 nm due to the formation of a cuprous bis-cysteine complex (RS–Cu^{1}–SR). EPR studies indicated that the metal stayed reduced during cysteine oxidation and only returned to its oxidized state once all the cysteine molecules had been converted to their oxidized form, RSSR. Under anaerobic conditions, Cu enhanced the reduction rate of compounds like ferricytochrome c (cyst c) and nitroblue tetrazolium (NBT) by cysteine, showing that the complex directly facilitated the reduction process. This RS–Cu–SR acted as a catalyst for cysteine oxidation.[104]

Cu–Rd from *Desulfovibrio gigas* was studied to help understand copper–cysteine redox chemistry. EPR spectroscopy revealed Cu–Rd's Cu(II) core with a sulfur-rich coordination, forming a deformed tetrahedral structure. Electrochemical studies showed that Cu–Rd's Cu core switched between Cu(II) and Cu(I) states during cysteine oxidation–reduction,

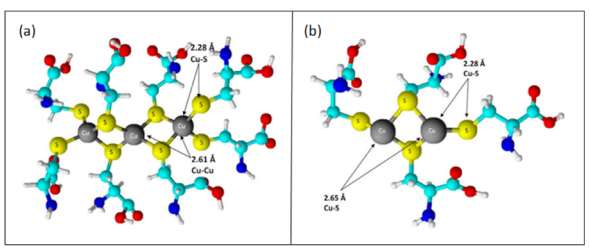

Fig. 6 Structure proposed for the Cu(II) : cyst complexes at (a) 1 : 2 and 1 : 6; (b) 1 : 4 mole ratios.

suggesting internal geometry rearrangements for electron transport. The midpoint potential of the [Cu^{I}(S–cyst)$_2$(cyst–S–S–cyst)]/[Cu^{II}(S–cyst)$_4$] redox couple was −0.15 V *vs.* NHE, indicating a significant separation between the cathodic and anodic peak potentials (ΔE_p = 0.575 V). Copper reduction and cysteine oxidation could proceed *via* oxidative or photochemical pathways. Under O_2, Cu^{II} acted as an electron carrier from cysteine to O_2, facilitating reduction at the Cu-center to yield Cu^{I}(S–cyst)$_2$(cyst–S–S–cyst).[86]

Rigo *et al.*[87] observed that cuprous ions bind strongly to the thiol group of cyst, resulting in polymeric species with bridging thiolate sulfur. At a ratio of 0.45 : 1, cysteine reduced cupric ions to Cu(I), resulting in the stoichiometric synthesis of cysteine. The excess cyst complexed the Cu(I) generated by this reaction. Excessive Cu(II) caused the cyst–Cu(I) complex to oxidize quickly and completely, resulting in the formation of Cu(0) precipitates. Cu(II) oxidized cyst–Cu(I) to produce aqueous Cu(I), which underwent dismutation and regenerated Cu(II). This method suggested that uncomplexed Cu(II) acted as a catalytic oxidative agent in the absence of molecular oxygen.

However, in this review article, we focus on the synergism of cysteine and copper, while copper is in a nanoregime. By employing the synergism between cysteine and copper particles, (nanoparticles/nanoclusters), various applications have been achieved. Besides, the synergism of cysteine and ionic copper has been employed to produce copper particles, where cysteine was a reducing and/or capping agent, enabling a myriad of applications (sensing, bioimaging analysis.). Such cysteine-capped copper particles have also been employed in natural samples in the context of environmental remediation.

Ahmed *et al.*[88] showed the sensitivity of cysteine detection *via* copper nanoparticles and observed the synergistic behavior of copper and cysteine. Copper nanoparticles showed a brown color, but in the presence of cysteine, they turned to olive green with a concomitant change in the SPR maximum. The selective sensing of cyst by CuPANs was confirmed by the color shift and total disappearance of the CuPANs SPR band in the presence of cyst. The thiol group of cyst's chemisorptions on the surface of CuPANs may be the cause of the disappearance of the SPR band. Other coexisting amino acids had minimal impact on cyst absorption. The CuPANs sensing platform only detected cyst in the mixes and was not sensitive to other amino acids [Fig. 7].

Xu *et al.*[89] modified a microcantilever with a self-assembled monolayer (SAM) of L-cysteine, resulting in a sensitive and selective response to Cu(II) ions in an aqueous solution. The microcantilever was bent as a result of Cu(II) ion sorption. The Cu(II) ions interacted with L-cysteine on the cantilever by diffusion, rather than by a straightforward Langmuir adsorption model. When the concentration of Cu^{2+} rose, the microcantilevers bent down faster. Higher [Cu^{2+}] (10^{-4} and 10^{-3} M) caused the cantilever to bend down faster and with greater amplitude. Cu^{2+} complexation at 10^{-3} and 10^{-4} M resulted in identical bending rates and amplitudes, indicating that Cu^{2+} sorption on the L-cysteine monolayer had achieved its maximum. The L-cysteine-modified cantilever sensor was tested for selectivity to Cu^{2+} over other cations. Exposure to Na^{+}, K^{+}, Pb^{2+}, Zn^{2+}, Cd^{2+}, Ni^{2+}, and Ca^{2+} resulted in minimal microcantilever deflection at a mid-level test concentration (10^{-5} M). The results indicated that L-cysteine-modified microcantilevers could detect Cu^{2+} with good sensitivity and selectivity.

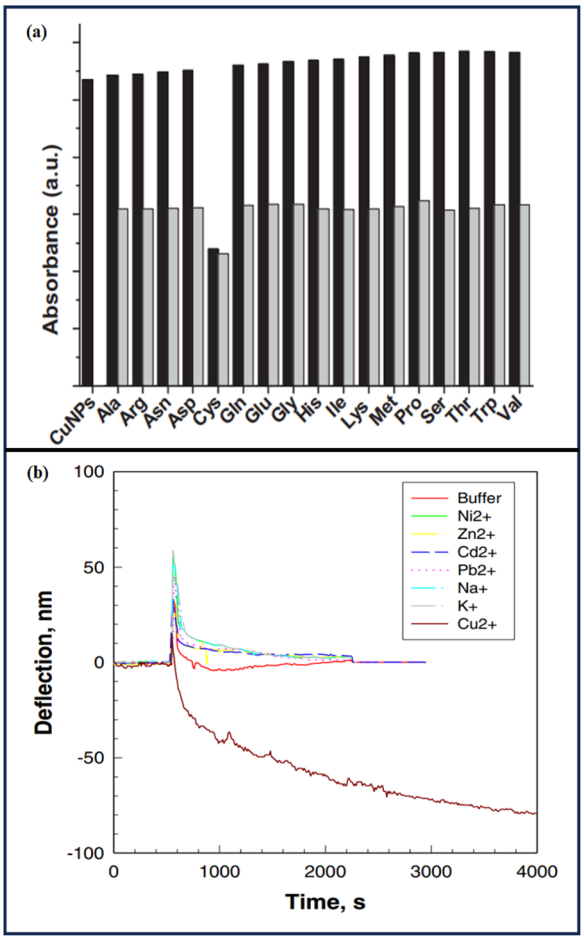

Fig. 7 (a) CuPANs' response to various amino acids; (b) bending deflection reaction to Cu^{2+} and other cations of a silicon cantilever coated with a self-assembled monolayer of L-cysteine on the gold surface.

Cysteine can efficiently cap copper nanoparticles and copper nanoclusters. Such cysteine-capped copper particles are utilized for versatile sensing applications. On the other hand, copper particles (NAPs and NACs) stabilized from other capping agents are used for sensing cysteine. In both cases, the interactions of cysteine and copper are crucial. No other amino acid can have so a pronounced effect with copper, as highlighted in the literature. Cysteine is a thiolated amino acid like methionine. However, reports of methionine are quite rare. Thus the synergism of cysteine and copper is quite evident and the driving factor of this review article.

6. Evolution of cysteine-passivated copper particles

Cyst as a capping agent plays a vital role in the stabilization of copper particles (NAPs and NACs). Cyst is mostly used as a capping as well as a reducing agent. However, there are reports

also in which cyst acts as a capping agent and ascorbic acid acts as a reducing agent.

6.1 Copper nanoclusters

Due to the metal's extreme oxidation susceptibility, ensuring atomically exact CuNAPs stability is a main concern. Over the past few decades, this stability issue has been substantially resolved by developing synthetic methods, employing mild situations, or picking suitable ligands with distinctive structures and elevated metal binding affinities[90–92] [Fig. 8].

6.1.1 Synthetic route. Table 1 list some reports and examples of the capping of cysteine to copper particles. However, poly-L-cyst has also been employed to cap copper particles. Specifically, to create a porous poly-L-cyst film-modified electrode (poly-L-cyst/GCE), a glassy carbon electrode (GCE) was dipped in an L-cyst aqueous solution and electrodeposited using cyclic voltammetry (CV) under potentials ranging from −4.5 V to 1 V at a rate of 100 mV s^{-1} for 15 cycles by Pan *et al.*[91] To incorporate Cu^{2+} *via* the Cu–S bond, the electrode was incubated with $CuSO_4$ solution for 10 min at room temperature. The resulting electrode was submerged in phosphate buffer saline for the *in situ* electrochemical reduction of Cu^{2+} with electrostatic deposition to produce CuNACs in the poly-L-cyst porous film (CuNACs/poly-L-cyst/GCE), which was then rinsed with deionized water to remove the uncombined Cu^{2+}. Moreover, the absorbent poly-L-cyst structure could offer plenty of accessible surface sites for concentrating CuNAPs inside the holes, which enhanced CuNACs steadiness and sped up electron transmission close to the electrode surface.

6.1.2 Applications

6.1.2.1 Sensing

6.1.2.1.1 Inorganic analytes. Alkaline phosphatase (ALP), a hydrolytic enzyme that is vital in cell signaling pathways, is measured as part of a standard blood test for assessing its activity.[92] Numerous photo/electric analytical techniques have been created to evaluate ALP. However, their sensitivity was typically constrained due to the absence of target amplification. CuNACs included in a poly-L-cyst film were used as the electrochemiluminescence luminophore. The poly-L-cyst served as a core action throttle in an electrochemiluminescence triple-structure complex (CuNACs/$S_2O_8^{-2}$/poly-L-cysteine) that produced an electrochemiluminescence biosensor with outstanding act for ALP sensing. As the quantity of ALP was enhanced from 10^{-8}–10^{-2} U L^{-1}, the biosensor's electrochemiluminescence signal grew. The electrochemiluminescence intensity and the log of ALP (LOD = 0.9984) concentration showed a desirable linear relationship. The detection limit was 9.5×10^{-7} U L^{-1} and the RSD was 1.1%. SEM imaging was utilized to examine the size and morphology of poly-L-cyst, as demonstrated by Pan *et al.*[91] It became obvious that the poly-L-cyst had a permeable film structure, scattering many stomates with diameters of roughly 100 nm on its surface. In the HRTEM images of CuNACs, the interplanar arrangement of the lattice fringes was 0.207 nm, corresponding to the (111) face-centered planes. The XPS plot showed two distinct peaks at 953.6 and 932.7 eV, corresponding to copper (0) $2p_{1/2}$ and $2p_{3/2}$, respectively. It was inferred that Cu^{2+} was absent in the CuNCl since there was no clear signal at 942 eV [Scheme 1].

Human serum solution (diluted 50 times by PBS) was added to the ALP solution at various concentrations for ALP detection. The recovery was determined from the ratio of the detected and real ALP concentrations [Table 2].

One of the most hazardous heavy metals in the environment is chromium(VI), which is recognized as highly carcinogenic to human lungs. While Cr(VI) is toxic to humans and organisms, trivalent chromium is a necessary nutrient for sustaining proper physiological function.[93–95] By using phosphate or sulfate transport mechanisms, Cr(VI) can easily enter cell membranes, where it can then undergo intracellular reduction, producing reactive intermediates, like chromium(V), chromium(IV), and oxygen radicals, that can lead to deoxyribonucleic acid mutation.[96,97] Among the contaminants caused by human activity, chromium poisoning of ecosystems comes in second as a cause of concern.[98]

Cui *et al.*[99] demonstrated a green approach for producing water-soluble luminous CuNACs using $CuCl_2$ and cyst as the precursor and stabilizer. In the presence of a low concentration of chromium(VI), the brilliant luminescence of CuNACs was efficiently quenched. The K_{sv} (Stern–Volmer constant) increased as the reaction temperature increased, showing that the increasing reaction temperature accelerated the effective collision and electron-transfer process among chromium(VI) and CuNACs. The luminescence excitation and emission bands of copper nanoclusters were not shifted when Cr(VI) was added. The luminescence intensity of CuNACs diminished proportionally as the [chromium(VI)] was increased from 0.06 to 60.0 μM. The system's dazzling green light gradually dimmed as the [chromium(VI)] concentration rose. The high oxidation state of chromium(VI) (LOD = 0.9981) should be responsible for such alterations, as any change in copper valence could result in structure breakdown and fluorescence quenching.

6.1.2.1.2 Organic analytes. ***6.1.2.1.2.1. Explosives.*** TNT (2,4,6-trinitrotoluene) has long been used in the military and mining areas. However, it can remain in the atmosphere and can cause a variety of health issues in humans and animals.[100] The fluorescence detection of TNT has been proven to be a sensitive and cost-effective technology. However, fluorescence quenching processes based on resonance energy transfer are unable to overcome the light bleaching inaccuracy.

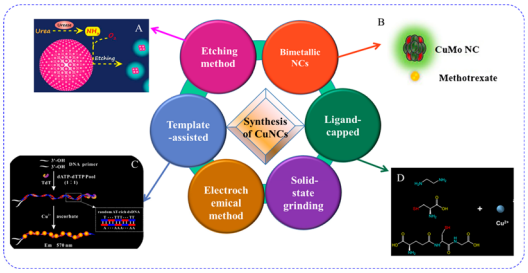

Fig. 8 Synthesis of copper nanoclusters.[92]

Table 1 Synthetic routes and properties of cyst-capped NACs

	Emission	Excitation	Stabilizing agent/etching agent	Reducing agent	Experimental conditions
Pan *et al.*[91] (2020)	—	—	Cysteine	Cysteine	Room temperature
Yang *et al.* (2017)[101]	500 nm	396 nm	Cysteine	Cysteine	Room temperature
Hambarde *et al.*[105] (2019)	492 nm	375 nm	Cysteine	Cysteine	45 °C on a water bath for 4.5 h
Lian *et al.*[130] (2021)	475 nm	368	Cysteine	Ascorbic acid	Ordinary temperature for 5 h
Borghei *et al.*[126] (2017)	425 nm	—	Cysteine	Cysteine	Room temperature
Anand *et al.*[135] (2019)	460 nm	360 nm	Cysteine	Cysteine	55 °C for 4.5 h
Sonaimuthu *et al.*[141] (2020)	492 nm	370 nm	Cysteine	L-Cysteine	Room temperature
Cui *et al.*[99] (2015)	490 nm	—	Cysteine	Cysteine	1.5 h at room temperature
Shanmugaraj *et al.*[106] (2018)	494 nm	370 nm	Cysteine	Cysteine	Room temperature
Li *et al.*[146] (2019)	497 nm	365 nm	Cysteine	—	2 h at room temperature

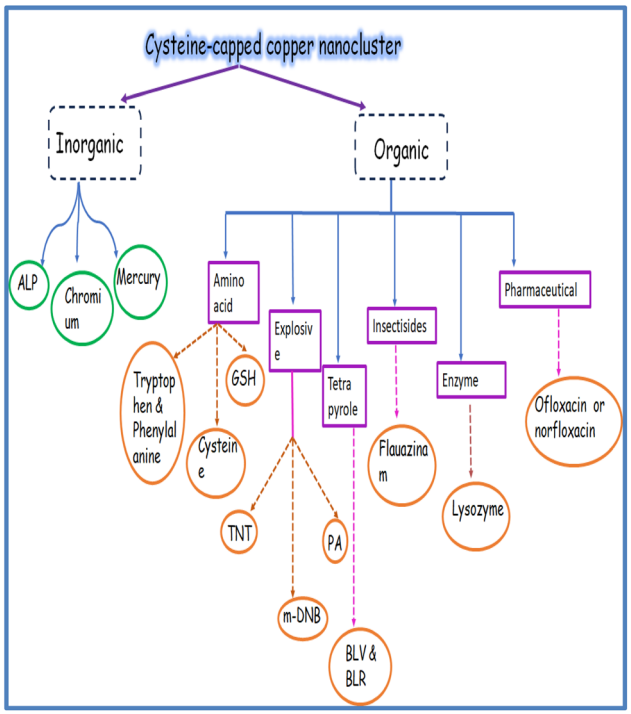

Scheme 1 Schematic representation of cysteine-capped copper nanoclusters as a sensing platform for various analytes.

Table 2 Human serum ALP actual sample analysis *via* an ECL sensor

Sample number	Added (U L^{-1})	Found (U L^{-1})	Recovery (%)	RSD (%)
1	1×10^{-4}	1.062×10^{-4}	106.2	0.6
2	1×10^{-5}	1.005×10^{-5}	100.5	2.1
3	1×10^{-6}	9.506×10^{-7}	95.06	2.4

Under 365 nm UV light, CuNACs aqueous solution emitted a weak fluorescence. The CuNACs were aggregated and emitted a strong olivine light with an emission peak red-shifted to 525 nm because of the donor–acceptor interaction, demonstrating that the CuNACs exhibited an aggregation-driven emission enhancement effect. The luminescence intensity of the copper nanocluster grew linearly as the TNT concentration increased. The correlation coefficient was more than 0.99, and TNT had a detection limit of 9.1 nM.[101]

The military sector uses nitro-aromatic (NA) compounds, such as picric acid (PA, *i.e.*, 2,4,6-trinitrophenol), *m*-dinitrobenzene (*m*-DNB), and others to manufacture volatiles, firecrackers, rocket-fuels, rawhide, and in ore mining, among other things. Regardless of their potential applications, the abuse, free dumping, and liberation of these NA compounds without post-processing can have major consequences for the environment and human health. PA's influence is significantly damaging, compared to all nitro-aromatics owing to its significant volatility and water solubility. PA pollution can potentially harm the kidneys, urinary, cardiac, metabolism, liver, and central nervous system.[102–104]

Hambarde *et al.*[105] demonstrated the simple and low-cost production of CuNAPs, using L-cyst-adapted CuNACs for the selective sensing of $-NO_2$-aromatic chemicals. The luminescence of the CuNACsCyst was reduced in the presence of PA owing to the inner-filter effect (IFE).[106] When m-dinitrobenzene (DNB) was added to the other investigated nitro-compounds, the fluorescence of CuNACsCyst was considerably increased and red-shifted from 492 nm to 525 nm. In the presence of m-dinitrobenzene, the luminescent color changed from bluish-green to green, whereas it became nonfluorescent in the presence of PA. With increasing m-dinitrobenzene concentrations, the luminescence intensity was enhanced linearly from 1.30×10^{-6} to 9.90×10^{-8} M, and the LOD was 1.3×10^{-7} M. The addition of PA marginally hampered the sensing of meta-dinitrobenzene by CuNACsCyst, although despite the slaking effects of PA on CuNACsCyst's luminescence, a noticeable fluorescent color alteration and turn/on luminescence increments were obtained.

When CuNACsCyst was exposed to *m*-DNB, the fluorescence was red-shifted and increased. Dynamic light scattering analysis was performed, and showed the formation of large aggregates of CuNACsCyst, suggesting the donor–acceptor interaction among meta-dinitrobenzene and CuNACsCyst (leading to a reduction in the inter-NCs distance and the creation of greater aggregates of

CuNACsCyst). Based on the aggregation-induced emission (AIE) process, CuNACsCyst was used to detect the selective luminescence turn/on of meta-dinitrobenzene.[107]

The fluorescence intensity of CuNACsCyst in the water sample could not be changed by direct analysis. Thus, several known quantities of *m*-DNB were spiked, and the recovery percentage was estimated from the calibration curve [Table 3].

Picric acid is a NA volatile organic substance that is extensively utilized in the production of fireworks, forensic inquiries, pharmacological, military, and dye sectors.[108,109] It has a more fierce and greater volatile nature than TNT due to its quick explosion velocity and low-security coefficient.[110] Due to its remarkable solubility in water, and extensive use in a variety of industries, it is considered a serious pollutant of soil, aquatic, and groundwater systems after exposure. It can cause damage to the kidneys, liver, metabolism, male infertility, and lead to anemia, cyanosis, and cancer.[111,112] Picramic acid, which has been observed to be 10 times more mutagenic than picric acid, is produced when picric acid travels up the food chain to the digestive systems of animals.[113,114] PA levels in drinking water are limited to 0.5 mg L^{-1}, with a satisfactory-regular-intake (SRI) of 1–37 gm.[115]

The IFE is commonly regarded as a mistake in luminescence measuring. Because of its simplicity, versatility, and significantly improved sensitivity and selectivity, IFE has received a lot of interest in the sensor sector. IFE can occur when an analyte's absorption spectrum overlaps with the λ_{ex} or λ_{em} spectral signals of luminophores. The IFE-based sensor design is supple, as it does not necessitate the shallow alteration of metal NACs or the formation of any covalent connection among the receptors and luminophores.[116]

Shanmugaraj *et al.*[106] used green luminous CuNACs to demonstrate the sensing of PA in aquatic solutions. Cyst behaved as a steadying and RA in the CuNACs' synthesis. PA greatly inhibited the luminescence of the as-synthesized CuNACsCyst, owing to the synergetic impact of IFE and the results from the static slaking method. In the absence of picric acid, CuNACsCyst exhibited a maximum luminescence at 494 nm when excited at 370 nm. The luminescence intensity at 494 nm was reduced when 2.5 μM PA was added to CuNACsCyst. As the [PA] was increased from 560 μM, the luminescence intensity of CuNACsCyst at 494 nm dropped consecutively without any shift in the overall emission wavelength. The luminescence intensity was reduced by approximately 81% after the accumulation of 60 μM PA, and the luminescence of CuNACsCyst was eliminated after the accumulation of 250 μM PA. The detection range of PA was 2.5–25 μM with a limit of detection of 0.19 μM.

The potential practical use of the current fluorescent probe in the detection of PA in water samples was investigated. A recovery investigation was carried out with samples that had been spiked with common PA solutions (10 and 25 μM) [Table 4].

6.1.2.1.2.2 Amino acids. Cyst has a strong affinity for Cu ions, which makes it possible to synthesize CuNACsCyst with outstanding photophysical characteristics. The size of the produced NACs is mostly determined by the ocular characteristics of CuNACsCyst, which is mainly reliant on [cyst].

For various cyst concentrations, the UV-vis absorption spectra of CuNACsCyst showed peaks at ~410 nm, 440 nm, and 580 nm respectively. The outcomes most likely showed that the bigger CuNAPs had been effectively transformed into lesser CuCuNACs. Due to cyst's protection, the resulting CuNACsCyst also showed high dispersion and no aggregation. Even though cyst is an AA, it exists as a zwitter ion and exhibits bands typical for primary amine and carboxylate salts. These bands correspond to very broad (NH^{3+}) stretching, asymmetric/symmetric (–NH) bending, and asymmetric/symmetric carboxylate ion (–COO) stretching. As the [cyst] increased from 60 μM to 500 μM with detection limits of 2.4 μM and 60 μM, the CuNACsCyst fluorescence intensity decreased correspondingly. Scanning electron microscopy images of the NACs in the three different [cyst] forms demonstrated the altered shape and increased size of the NACs as the cyst concentration increased. The hydrodynamic diameters of CuNACsCyst, about [cyst], varied roughly from 2.5 to 20 nm, respectively[117] [Fig. 9].

The detection of cyst in actual serum was also performed in order to assess the usefulness of the proposed nanobiosensor for biological samples. The cyst concentrations were elevated. Additionally, the recovery test was performed by adding various doses of cyst to serum samples [Table 5].

The chemiluminescence (CL) approach has evolved into a valuable and strong tool in a variety of analytical domains, including bio-technological, ecological, food, and pharmaceutical analysis.[118,119] The application of CL is limited owing to the low chemiluminescence intensity of numerous systems. Conservative fluorophores have been introduced in recent years to improve the chemiluminescence intensity and sensitivity.[120,121] Amino acids have been identified as possible indicators of cancer and as precursors of a variety of important biological molecules.[122] In particular, L-tryptophan is one of the greatest essential AAs found in natural proteins, and it is widely employed as an antioxidant in the food business and as a biomarker in pharmacological manufacturing. Furthermore,

Table 3 Measurement of *m*-DNB in tap water from the real sample analysis of CuNACsCyst

Sample	Added	Found	Recovery %
Tap water	3.85×10^{-7}	3.26×10^{-7}	84.8
	1.07×10^{-6}	8.90×10^{-7}	83.0
	5.66×10^{-7}	4.83×10^{-7}	85.4

Table 4 Estimation of [PA] in several water samples

Samples	Amount of PA spiked (μM)	Amount of PA found (μM)	Recovery (%)	RSD (%) ($n = 3$)
1	10	9.8	98	3.17
2	25	24.8	99.2	1.14
3	10	9.7	97	2.96
4	25	24.6	98.4	1.95

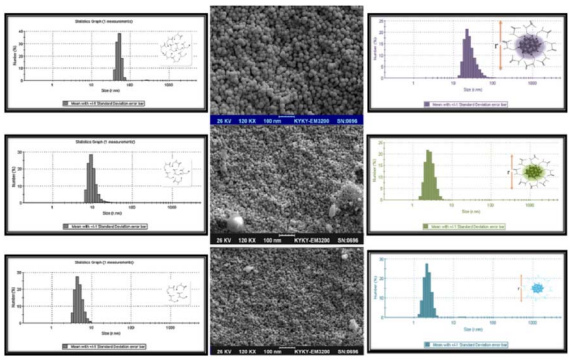

Fig. 9 CuNACs detection at various cys concentrations as seen using SEM, (Inset): CuNACs size-distribution analysis (1, 100, and 10 μM cyst).

it plays a crucial part in a variety of biological processes.[123] Both trp. and phenylalanine are required amino acids in the human diet. Tyrosine, a non-essential amino acid, is produced by phenylalanine. Womack and Rose discovered the synthesis of tyrosine from phenylalanine in 1934. This conversion is catalyzed through phenylalanine hydroxylase, which is found primarily in the liver but has also been found to be present in the kidney, pancreas, or brain.[124,125]

Borghei *et al.*[126] demonstrated that CuNACsCyst could be easily made by employing cyst as the template, precursor, and stabilizer. They discovered that CuNACsCyst could improve the chemiluminescence of the luminol–H_2O_2 scheme and that under the right conditions, tryptophan and phenylalanine might improve the chemiluminescence of this NACs-boosted system even more. They observed that phenylalanine and tryptophan increased the chemiluminescence intensity of the luminol–H_2O_2–CuNACs reaction scheme significantly; whereas other AAs did not affect the luminol–H_2O_2–CuNACs reaction system. The calibration plots for tryptophan were linear throughout a range of 1×10^{-7} to 3×10^{-5} M, ($r^2 = 0.98$). A comparable calibration curve for phenylalanine was shown, with a linear range of 1×10^{-6} to 2.8×10^{-5} M ($r^2 = 0.96$). The detection limits for tryptophan and phenylalanine were 7.6×10^{-8} and 8.3×10^{-7} M, respectively. For 10 μM phenylalanine and 5 μM tryptophan, the RSD ($n = 5$) were 1.5% and 3.3%, respectively.

The suggested method's applicability was evaluated by measuring tryptophan and phenylalanine levels in human serum samples. The plasma samples were then spiked with equal concentrations of tryptophan and phenylalanine (10 and 20 μM) [Table 6].

Zhang *et al.*[127] established a luminescence detector (L-cyst/CuNACs @ eggshell membrane) using an *in situ* method, with

Table 6 Tryptophan and phenylalanine levels in serum samples

Sample	Added (μM)	Found (μM)	Relative error (%)
Tryptophan	10	9.5a ± 0.3	5
	20	19.3 ± 0.4	3.5
Phenylalanine	10	9.6 ± 0.5	4
	20	—	4

L-cyst acting as a reducing and protective agent for Hg(II) and glutathione (GSH) visual detection. The as-prepared luminescent product demonstrated excellent steadiness, and movability, as well as a substantial Stokes shift (250 nm) and long luminescence life-time (7.3 ms). The L-cyst/CuNACs @eggshell membrane demonstrated a distinct luminescence slaking response to mercury(II). Furthermore, the interaction of GSH with mercury(II) could efficiently recuperate the luminescence. Hg^{2+} had a detection limit of 1.1 μM for visualization and 0.52 μM for the luminescence spectrometer. GSH had similar limits of detection of 2.8 and 0.59 μM, respectively.

6.1.2.1.2.3 Pharmaceuticals. One of the most potent synthetic antibiotics known is quinolone (QN), which has broad-spectrum bactericidal activity against both Gram-positive and Gram-negative bacteria.[128] It is significant in human health, diet security, and animal agriculture manufacture due to its broad antibacterial range, high oral absorption, and inexpensive cost. The majority of QNs given to people and animals are eliminated intact in feces and urine.[129] The development of simple and sensitive sensing technology for quinolones would be of tremendous importance and have significant application potential.

Lian *et al.*[130] developed a special luminescent detection method for quinolones sensing based on luminescence turn/on inflection. Cyst-stabilized CuNACs were created by core etching nonfluorescent CuNAPs with excessive cyst. Ofloxacin (OFX) or norfloxacin (NOX) were chosen as QN models. Because of the interaction of Fe^{3+} and CuNACsCyst, the luminescence of the as-prepared CuNACsCyst were effectively slaking in the presence of iron(III). However, after adding quinolones to the slaking system, the luminescence of the CuNACsCyst system was significantly reinstated owing to the robust coordination among iron(III) and the quinolones. They discovered that when CuNACsCyst was mixed with ofloxacin, the luminescence spectra remained identical to the original, but the luminescence intensity was marginally increased, indicating that ofloxacin had a small sensitization impact on CuNACsCyst's luminescence. The pH had an impact on complex formation as well; complexes were steadier at lower pH. The first dissociation

Table 5 Recovery of cyst in serum samples spiked with CuNACsCyst

Serum	Original ($nmol^{-1}$)	Added ($nmol^{-1}$)	Found ($nmol^{-1}$)	Recovery (%)	RSD (%, $n = 3$)
1	4.2	10	13.6	94	3.6
2	8.4	10	18.7	103	1.8
3	10.3	10	20.1	97	2.3

constant (DC) of quinolones (pK_{a_1}) refers to proton dissociation (PD) from the –COOH, and the second DC (pK_{a_2}) corresponds to PD from the piperazine group's N-4′.

Because of the existence of –COOH and alkaline piperazinyl groups, QNs are zwitter-ionic. They could be present in solution as cations, neutrals, anions, and zwitterions, contingent on the pH of the solution and the DC. The affinity of quinolones for metal ions decreases in the order of anion, zwitterion, and cation.[131] In the concentration ranges of 0.5–40 micromolar and 0.5–50 μM, the luminescence intensity was compared to that of [OFX] and [NOX]. OFX and NOX both had detection limits (S/N = 3) of 50 nM. The R^2 of OFX and NOX were 0.998 and 0.998, respectively.

Lian *et al.*[130] established a method to detect OFX and NOX in fresh human urine samples. The recoveries for OFX and NOX ranged from 97.80–101.80% and 97.20–102.30%, respectively [Fig. 10].

6.1.2.1.2.4 Tetrapyroles. Biliverdin ($C_{33}H_{34}N_4O_6$) [BLV] and bilirubin ($C_{33}H_{36}N_4O_6$) [BLR], two naturally occurring vitriol pigments, are linear tetrapyrroles that are created during heme catabolism.[132,133] In the presence of heme oxygenase, heme is oxidatively destroyed to create BLV, which will thereafter shortly be reduced to BLR by the enzyme BLV reductase. In adults, an excess of BLR causes hyperbilirubinemia, which can lead to major health problems, such as mental disorders, liver ailments (cirrhosis, hepatitis), and, in extreme circumstances, even death. A low level can cause anemia and coronary artery disease.[134]

Using naturally occurring aminothiol L-cyst-stabilized CuNACs, Anand *et al.*[135] presented a simple, precise, and economical technique for the selective measurement of biliverdin and bilirubin. Through static mechanisms, biliverdin and bilirubin both reduced the luminescence intensity of CuNACsCyst. The size that was achieved was within the cluster range and the particles were monodispersed. It was discovered that the L-CuNACsCyst hydrodynamic diameter was 5.6 nm, which was consistent with the findings of the TEM investigation. For BVD and BLR, it was discovered that the fluctuation in relative fluorescence intensity (I_0/I) with the concentration increase was linear in the ranges of 4×10^{-5} to 5×10^{-7} M and 1.00×10^{-5} to 1.00×10^{-6} M, respectively. The LOD for biliverdin and bilirubin were 2.3×10^{-7} M and 2.30×10^{-7} M, respectively.

Spike recovery analysis was used to measure the amount of BVD/BLR in artificial blood serum and urine samples to assess the effectiveness of the proposed sensor [Table 7].

6.1.2.1.2.5. Enzymes. LYZ (Lysozyme) has been widely utilized as a model protein in amyloid, crystallography, and nanomaterials research.[136,137] Lysozyme is found in both eukaryotes and prokaryotes and is divided into three types: poultry (type c), goose (type g), and invertebrate (type i).[138,139] Lysozyme can destroy the shielding cell-ramparts of usual micro-flora, shielding humans from the threat of microbial contagion. Its aberrant concentration in blood and urine is linked to a variety of illnesses, including leukemia, kidney disease, and meningitis, and it has been employed as a biomarker.[140]

Sonaimuthu *et al.*[141] reported L-cyst-protected ultra-tiny CuNCl coupled with β-cyclodextrin (CD) for the quick sensing of lysozyme in human serum samples at ambient temperature. The CuNACs were synthesized with the inclusion of β-CD throughout the synthesis, which resulted in a higher emission intensity. This might be a result of the enhanced charge transfer occurring between CuNACs and β-CD. Cysteine and β-CD exhibited no discernible luminescence or peak, pointing to the development of luminescence NACs[142,143] [Table 8].

6.1.2.1.2.6. Insecticides. The luminescence slaking processes of luminophores in the existence of numerous analytes, including fluorescence resonance energy transfer (FRET), IFE, creation of a donor–acceptor charge-transfer complex, and static and dynamic slaking effect. To control outbreaks of late blight in agriculture, fluazinam, a phenylpyridinamine insecticide, is frequently employed.[144] Fluazinam has a lasting effect on crops and is challenging to remove.[145]

Li *et al.*[146] developed a label-free luminescent probe based on CuNACs that had been L-cyst adapted to sense fluazinam. L-cysteine and $CuSO_4$ were used as the building blocks for the synthesis of L-CuNACsCyst. Fluazinam displays a UV-vis absorption peak at 352 nm, while L-CuNACsCyst had λ_{ex} and λ_{em} peaks at 365 and 497 nm, respectively. Fluazinam's absorption band greatly overlapped the luminescence stimulated and emitted wavelength of L-CuNACsCyst, allowing fluazinam to absorb and shield a portion of the λ_{em} and λ_{ex} luminescence of L-CuNACsCyst. Fluazinam concentration in the range of 0.05–25 μM revealed a solid linear relationship, with an LOD of 1.4 nm (R^2 0.995).

A fluorescent probe based on IFE was used to determine fluazinam in pears and cabbages to assess its feasibility and application in real samples. The pears and cabbages were spiked with a variety of fluazinam concentrations (1, 5, 10 ppm) [Table 9].

6.1.3 Bimettalic clusters. Methotrexate (MTE) is an antineoplastic medication used to treat a variety of malignancies. It works by inhibiting dihydrofolate reductase, an enzyme necessary to produce nucleotides.[147] It is the first-line treatment

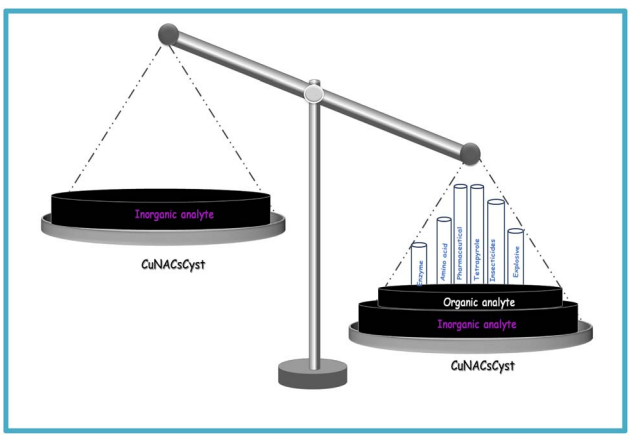

Fig. 10 Copper particles used with cysteine.

Table 7 BLV and BLR determination in artificial blood serum and urine samples

		Proposed method			Standard method		
Sample	Added	Found (M)	Recovery (%)	RSD	Found (M)	Recovery (%)	RSD
Blood serum	BVD 4.00×10^{-5} to 5.00×10^{-6}	4.23×10^{-5} to 5.23×10^{-6}	102	4.68	3.92×10^{-5} to 5.33×10^{-6}	101	4.39
	BLR 1.00×10^{-5} to 1.00×10^{-6}	9.95×10^{-6} to 1.01×10^{-6}	95	3.72	9.86×10^{-6} to 1.01×10^{-6}	102	2.60
Urine	BVD 3.00×10^{-5} to $4.00\ 10^{-6}$	3.20 × 10-5 to 3.99 × 10-6	102	3.51	2.98×10^{-5} to $4.47\ 10^{-6}$	105	4.31
	BLR 1.00×10^{-5} to $1.00\ 10^{-6}$	9.70×10^{-6} to 1.02×10^{-5}	101	3.12	9.59×10^{-6} to 9.57×10^{-7}	99	3.90

for people with rheumatoid arthritis who have not been able to control their condition well enough with nonsteroidal anti-inflammatory drugs.[148] MTE doses as high as 500 mg m^{-2} can be used to remedy all types of osteogenic sarcoma and lymphoma in both adults and infants. As a cytotoxic chemical, MTE affects not only cancerous cells, but also healthy cells and organs.[149]

HRTEM images indicated the absence of a core–shell structure in bimetallic NACs, indicating the production of alloyed NACs. The copper/molybdenum NACs lattice spacing was 0.38 nm. That contrasts with the lattice spacings of Cu (0.36 nm) and Mo (0.31 nm). Copper had a redox potential (RP) of 0.34 V and an atomic radius of 1.28 Å, while molybdenum had an RP of −0.15 V and an atomic radius of 2.08 Å.[150] When MTE was steadily introduced to copper/molybdenum NACs, the associated fluorescence intensities decreased as the concentration increased up to 100 μM. The linear responses of the luminescence intensity with MTE concentrations ranged from 0.05–100 M, $R^2 = 0.9857$. The detection limit was set at 13.7 nM.[151]

When a healthy person's blank urine sample was applied to the sensing system, there was no noticeable fluorescence reaction, which suggests that human urine did not significantly affect the device's performance. Around 99% of the MTE was recovered from spiked human urine [Table 10].

6.2 Copper nanoparticles

6.2.1 Synthetic route. In a synthetic approach, de-ionized water was used to dilute a 300 μL solution of copper chloride at 0.003 M. This was then mixed with 20 μL of a 0.01 M L-cyst solution, which changed the mixture's light blue tint to colorless. Next, 1000 μL of 0.1 M hydrazine monohydrate was added for the reduction of metal ions, and within 60 min reaction, the solution mixture turned crimson. According to the L-cyst pK_a values, the pH of the entire mixture was kept at 6 to obtain the lowest particle size.

Table 9 Fluazinam concentrations in spiked samples

	Spiked (ppm)	Found (ppm)	RSD (%)	Recovery (%)
Pears	1	1.042	4.20	104.20
	5	5.066	1.32	101.32
	10	10.042	0.42	100.42
Cabbages	1	0.994	0.60	99.40
	5	4.946	1.08	98.92
	10	10.463	4.63	104.63

6.2.2 Applications

6.2.2.1. Sensing. Mercury is regarded as one of the most harmful metals in the form of mercury(II) ions for the atmosphere and for human beings due to its widespread dispersion in numerous metallics and organic and inorganic forms present in air, water, and soil.[152–154] Because of its increased aquatic solubility, mercury(II) ions are regarded as the greatest stable form of inorganic Hg, which may effortlessly persist in surface waters and may cause a variety of health problems, including brain, kidney, and nervous system damage.[155,156]

Due to the localized surface plasmon resonance band spectrum of CuNAPs, which is in between 400 and 600 nm, the colloidal sol of these particles has a brick red color. The narrow band shape of the distinctive LSPR band, which has a wavelength of 565 nm, confirms the aqueous medium's crystalline makeup. LSPR is a straightforward measurement of an λ_{ex} (λ_{em}-scattering) peak shift or change, like surface plasmon resonance, which is sensitive to changes in bulk refractive index close to the metal particle surface, leading to a shift in resonance angle. In response to the interaction of CuNAPsCyst with mercury(II) ions, a colorimetrical shift from brick red to pale yellow was observed. This change in color was correlated with a shift in the spectrum profile of CuNAPsCyst from a narrow, blue-shifted band to a larger, red-shifted spectrum with reduced intensity. Based on particle aggregation in the aqueous

Table 8 Use of a synthetic β-CD-CuNACs probe to detect LYZ in human serum samples

Serum samples	Concentration added (μM)	Concentration found (μM)	Recovery (%)	RSD (%) ($n = 3$)
1	30	28.84	96.15	2.75
2	50	49.83	99.67	0.51
3	70	70.99	101.42	1.71
4	90	93.64	104.05	0.79
5	100	103. 48	103.48	1.38

Table 10 Recovery of MTE in human urine

Sample	MTX added (μM)	MTX measured (μM)	Recovery ($n = 3$, %)
Human urine	20	19.9	99.5
	36	36.1	100.2

solution, a change in spectral character upon exposure to mercury(II) was observed.[157]

The CuNAPsCyst particles that were produced in the absence of Hg^{2+} were well dispersed and spherical, with an average particle size of 34 ± 72.1 nm and a range of 10–108 nm, according to the TEM image. The interaction of the biomolecule L-cysteine with the surface of the CuNAPs was sufficient to produce stable, spherical NAPs.

The alterations in the Δ*A* (localized surface plasmon resonance) band of CuNAPsCyst in the 400–800 nm spectral region were caused by adding Hg^{2+} ions. The method demonstrated good linearity in the calibration range of 0.5×10^{-6} to 3.5×10^{-6} mol L^{-1} of Hg^{2+} ions. The R^2 was 0.988, and the LOD and LOQ were 4.31×10^{-8} and 0.1×10^{-a} mol L^{-1}, respectively.

The developed sensor based on the localized surface plasmon resonance of CuNAPsCyst was used to determine the presence of mercury(II) ions in aquatic samples from several locations along the River Sindh near the Kotri Barrage. The samples were handled after being properly diluted to bring the final concentration of mercury(II) ions within the sensor's linear range.

7. Copper nanoclusters for cysteine sensing

7.1 Synthetic route

Copper sulfate solution with a concentration of 10×10^{-3} mol dm^{-3} was combined with glutathione solution to generate CuNACs. The clear solution turned into a white suspension liquid. Then, when the color of the solution changed from a turbid liquid to a visible bright yellow and the equivalent pH value was 4–5, 1 mol dm^{-3} concentration of sodium hydroxide was added dropwise. This mixture was rapidly agitated for h at a temperature of 37 °C.

7.2 Applications

7.2.1. Sensing. Ma *et al.*[158] synthesized and integrated silicon quantum dots (SiQDs) and glutathione-steadied CuNACs as a ratiometric luminescent probe for L-cyst testing in milk. CuNACs diminished the luminescence of SiQDs *via* a fluorescence resonance energy-transfer process. The 440 nm luminescence of SiQDs showed an insignificant change when L-cyst was added, whereas the 650 nm fluorescence of CuNACs was decreased significantly. In the [L-cyst] range of 0.25 μM to 2.5 mM, the ratiometric fluorescence signal was linear, with a detection limit of 75 nm and a visible color change from red to blue.

Thiol functional groups have been utilized to alter and stabilize metallic NACs because they interact strongly with metal atoms. GSH-stabilized metal NACs have found applications in several industries. Functional groups like carboxyl, thiol, and amino groups can be found in glutathione (GSH) tripeptide (glu–cyst–gly).[159]

Glutathione–CuNACs had a maximum emission wavelength of 613 nm and an exciting wavelength of 380 nm. With the gradual increase in cyst, the emission intensity of the GSH@-CuNACs decreased gradually. In this assay, the tiny biothiol molecule (cysteine) was broken in the glutathione protective layer of GSH@CuNACs, influencing the NACs surface *via* the formation of a metal–thiol complex, which was primarily related to the slaking of the glutathione@CuNACs emission. The emission intensity of GSH@CuNACs decreased gradually with the increment in the [cyst], reaching about 89% at 3×10^{-8} mol dm^{-3} cyst, whereas no significant λ_{em} shift was detected. The λ_{em} of the glutathione@CuNACs was significantly reduced with the accumulation of 45×10^{-7} mol dm^{-3} of cysteine analyte. Various primary AAs and metal ions induced insignificant alterations to the λ_{em} of glutathione@CuNACs (LOD = 8.63×10^{-9} mol dm^{-3}).[160]

The small biothiol molecule (cyst) caused the GSH-CuNACs protective layer to break down in this assay, which then damaged the surface of the NACs by creating a metal–thiol complex, which was principally responsible for the quenching of the emission. The interaction among glutathione and CuNACs, including the 3 and 4 Cu atoms of the CuNACs with the GSH-containing thiol connection, was extremely strong in the absence of cyst and had very short bond lengths of 2.61 and 2.72 Å, respectively. The third copper atom of CuNACs with glutathione comprising the R–S bond was elongated to 3.58 during the interaction of cyst with the CuNACs, while the 4-copper atom of CuNACs with glutathione comprising the R–S bond disappeared. The formation of a new bond among cyst comprising the R–SH group interacted with a copper atom of CuNACs with a bond length of 3 [Fig. 11].

7.2.2 Bioimaging analysis. GSH@CuNACs have enormous potential in bioimaging studies due to their capable fluorescent properties, such as water solubility, great surface bioactivity, and biocompatiblity.[161] Rajamanikandan *et al.*[159] used a nanoprobe to detect intracellular cysteine in living cells to determine

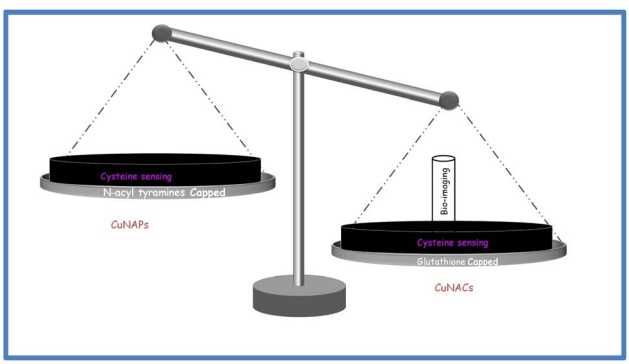

Fig. 11 Copper particles used for cysteine sensing.

the usability of GSH@ CuNACs. They observed that the nanoprobe was sensitive enough to distinguish the physiological intensity of cyst in cancer cells. The intracellular cell circulation and internalization of GSHCuNACs and glutathione@CuNACs were tracked using an optical fluorescence microscope and cellular imaging. They showed that HL-60 cell uptake exhibited intense red luminescence within cancer cells. That intense red luminescence behavior indicated that glutathione@CuNACs might be able to sense cyst in live cells. The variations in bright red luminescence in HL-60 cells after the accumulation of GSHCuNACs with cyst revealed that the cysteine level increased the luminescence properties.

7.3. Bimetallic (Cu/Ag) antibacterial activity of cysteine

Zhang *et al.*[162] used an easy and green UV photoreduction approach to create a unique and extremely stable cyst-directed Ag–Cu compound NACs hydrogel. The silver-CuNACs hydrogel was tested for its antibacterial effects on *Escherichia coli* (*E. coli*) and *Staphylococcus aureus* (*S. aureus*) utilizing growth curves, zones of inhibition, minimum inhibitory concentration, and minimum bactericidal concentration studies. The antibacterial activity of the AgCu NACs hydrogel against *E. coli* and *S. aureus* was found to be extremely synergistic, with minimum inhibitory concentrations of 0.78 and 3.12 μg mL^{-1}, and minimum bactericidal concentrations of 12.5 and 100 μg mL^{-1}, respectively.

7.4 Copper nanoparticles

7.4.1. Copper nanoparticles for cysteine sensing. Cyst is sparsely solvable in toluene compared to dichloro-diphenyl-trichloroethane, so it reduces copper(II) to copper(0) gradually, which was also reflected in the actual particle size. The synthesized CuNAPs showed a λ_{em} at 487 nm. The crosslinking of the ligand cyst to the metal surface, possibly catalyzed by the metal, may account for the solution's resistance to particle aggregation and interparticle interaction. A highly effective steric stabilization might explain the re-dispersible nature of the yellow solid and the inability of the mixable non-solvents to produce interparticle interaction. Uncertainty surrounds the specific nature of the crosslinking reaction, which may result from the coupling effect of the ligand cysteine.[163]

The average particle size, as shown by TEM, was 11.5 ± 0.5 nm. Only a minimal number of larger, spherical-shaped particles (~15.5 nm) were present, according to the TEM measurements, in addition to the evenly distributed microscopic particles. It could be seen that the particles had a limited size distribution from the particle size histogram. Dodecanethiol-protected CuNAPs were considerably smaller than cysteine-stabilized CuNAPs. It was discovered that the typical particle size was 8.6 ± 0.2 nm. The X-ray photoelectron spectroscopy measurement of the CuNAPs showed two peaks at 932.7 and 952.5 eV, corresponding to copper$(2p)_{1/2}$ and copper$(2p)_{3/2}$, respectively, which could be attributed to copper(0). No peak for the copper oxide or Cu_2O was found as such. The cysteine molecule's copper–sulfur bond could form an excellent barrier layer that shielded the Cu cores from oxidation.

Ahmed *et al.*[88] demonstrated a simple approach for producing CuNAPs by employing *N*-acyl tyramine (NLTA) as a covering agent and hydrazine as a reducing agent. A new class of multifunctional lipid effectors in the cannabinoid-vanilloid system called *N*-acyl dopamine was considered to have a precursor in the form of NLTA, a sort of fatty acid amide.[164] Another AA was added for selectivity assessment, but cysteine was the first one that induced a color shift in the CuNAPs from brown-olive green at the μM level. The absorbance peak of CuNAPs decreased with the increase in [cyst] and the R^2 value was 0.994. There was a good linear relationship between the absorbance intensity alteration and [cyst] over the range of 0–25 μM. The LOD was 0.10 μM and the LOQ was estimated to be 0.3365 μM.

According to Ahmed *et al.*,[88] the X-ray diffraction pattern of the synthesized CuNAPs revealed diffraction pattern peaks at 43.43, 50.58, and 74.38, which corresponded to the respective crystal planes (1 1 1), (2 0 0), and (2 2 0), respectively. The CuNAPs existed in a variety of morphologies, including spherical, prismatic, rod-like, pentagonal, and hexagonal patterns, as revealed by TEM. The existence of multifarious CuNAPs might be attributed to CuNAPs stabilization by distinct NLTA aggregation states. The size of the CuNAPs observed from the TEM images was 35–200 nm.

7.4.2 Bimetallic nanoparticles. Anions are found everywhere in the environmental loop, from Mother Nature to everyday human life. Significant development has been achieved in the domain of anions sensing and recognition over the last decade, as the sensing of anions can not only give a means of inspecting the atmosphere and testing aquatic water quality but can also aid in the biological identification of certain disorders. They can also provide an alternate viewpoint to investigate biological aspects through the roles that anions play in the human body.[165]

Zhang *et al.*[166] demonstrated the progress of an alternate sensitive and selective colorimetrical sensing system for sulfide anions utilizing Cu–AuNAPs cyst. Iodide could cause a considerable color shift of the Cu–AuNAPs solution from purple to red in the absence of sulfide anions or cysteine by changing the NAPs clusters to solitary, nearly spherical, and bigger ones. The selectivity was detected in the presence of another 19 natural AAs (10 μM) against cyst (1 μM) and revealed that the colorimetrical system had satisfactory selectivity toward cyst, with histidine and arginine being the first and second largest interferences, and the others being insignificant, including the sulfur-containing methionine. In the response range of 0–1.5 μM, a linear relationship was observed, with an LOD of 50 nM.

8. Conclusions

The dual aspects of copper particles (nanoparticles and nanoclusters) were summarized in the context of cysteine. Cysteine has been proven to be a unique capping agent as well as a reducing agent for copper nanoparticles and nanoclusters with sensing and bioimaging applications. Sometimes reducing agents, namely ascorbic acid, might be employed while cysteine

caps the particles. Stable copper particles passivated by other reducing agents were also summarized here for the selective and sensitive detection of cysteine. Thus, the synergism of cysteine and copper particles is of immense value. The role of amino acids in modifying the surface of particles provides hints for surface manipulation. This review hopefully opens up a new window for researchers in the field of nanoscience and optical devices. Real sample analyses bring a new fragrance for practical applications in environmental and physiological fields.

Conflicts of interest

There are no conflicts to declare.

Notes and references

1 M. I. Griffin, M. J. Masood, M. Nasim, A. P. Sarfraz, K.-H. Schäfer, C. M. Keck and C. Jacob, *Antioxidants*, 2018, **7**, 3.
2 J. F. Petty, M. Ganguly, A. I. Yuans, C. He, P. M. Goodwin, Y.-H. Lu and R. M. Dickson, *J. Phys. Chem. C*, 2018, **49**, 28382–28392.
3 Nanoparticle classification, physicochemical properties, characterization, and applications: a comprehensive review for biologists.
4 M. Brack, *Rev. Mod. Phys.*, 1993, **65**, 677.
5 Nanotechnology-Enabled Biosensors: A Review of Fundamentals, Design Principles, Materials, and Applications.
6 H. Bönnemann and K. S. Nagabhushana, Metal nanoclus ters: synthesisandstrategies for their size control, in *Metal Nanoclusters in Catalysis and Materials Science*, ed. B. Corain, G. Schmid and N. Toshima, Elsevier B.V., New York, NY, USA, 2008, ch 2, pp. 21–48.
7 M. Ganguly, J. Pal, S. Das, C. Mondal, A. Pal, Y. Negishi and T. Pal, *Langmuir*, 2013, **29**, 10945–10958.
8 J. D. Aiken III, Y. Lin and R. G. Finke, *J. Mol. Catal. A: Chem.*, 1996, **114**, 29–51.
9 A Comprehensive Analysis of Luminescent Crystallized Cu Nanoclusters.
10 S. Gulati, M. Sachdeva and K. K. Bhasin, *AIP Conf. Proc.*, 2018, **19**, 030214.
11 S. O. Aisida, A. Batool, F. M. Khan, L. Rahman, A. Mahmood, I. Ahmad, T.-K. Zhou, M. maaza and F. I. Ezema, *Mater. Chem. Phys.*, 2020, **255**, 123603.
12 S. O. Aisida, M. H. Alnasir, S. Botha, A. K. H. Bashir, R. Bucher, I. Ahmad, T.-K. Zhou, M. maaza and F. I. Ezema, *Eur. Polym. J.*, 2020, **132**, 109739.
13 S. O. Aisida, E. Ugwoke, A. Uwais, C. Iroegbu, S. Botha, I. Ahmad, T.-K. Zhou, M. maaza and F. I. Ezema, *J. Polym. Res.*, 2019, **26**, 225.
14 K. Rajendran and S. Sen, *Der Pharm. Lett.*, 2015, **7**, 37–42.
15 R. Javed, M. Usman, S. Tabassum and M. Zia, *Appl. Surf. Sci.*, 2016, **386**, 319–326.
16 Z. Niu and Y. Li, *Chem. Mater.*, 2014, **26**, 72–83.
17 I. A. Radini, N. Hasan, M. A. Malik and Z. Khan, *J. Photochem. Photobiol., B*, 2018, **183**, 154–163.
18 R. Javed, M. Zia, S. Naz, S. O. Aisida, N. ul Ain and Q. Ao, *J. Nanobiotechnol.*, 2020, **18**, 7.
19 P. Sharma and M. Ganguly, *New J. Chem.*, 2023, **47**, 7481–7485.
20 M. Sahu, M. Ganguly and A. Doi, *ChemistrySelect*, 2023, **8**, e202301017.
21 M. R. Willner and P. J. Vikesland, *J. Nanobiotechnol.*, 2018, **16**, 1–16.
22 P. Sharma and M. Ganguly, *Int. J. Environ. Sci. Technol.*, 2023, **21**, 3345–3364.
23 A. E. Harper, *J. Nutr.*, 1959, **68**, 405–418.
24 P. Li, Y.-L. Yin, D. Li, S. W. Kim and G. Wu, *Br. J. Nutr.*, 2007, **98**, 237–252.
25 A. Amiri-Sadeghan, A. Dinari, S. Mohammadi, T. Zohrabi, R. Khodarahmi, S. Hosseinkhani and J. Yoon, *Sci. Rep.*, 2022, **12**, 2235.
26 S. Saisree, V. Dhrishya and S. K. Yesodha, *ACS Appl. Nano Mater.*, 2022, 9404–9414.
27 W. Wang, Z. Wang, D. Sun, S. Li, Q. Deng and X. Xin, *Nanomaterial*, 2022, **12**, 424.
28 B. R. Khalkho, R. Kurrey, M. K. Deb, K. Shrivas, S. S. Thakur, S. Pervez and V. K. Jain, *Heliyon*, 2020, **6**, e03423.
29 J. Athilakshmi, M. Mohan and D. K. Chand, *Tetrahedron Lett.*, 2013, **54**, 427–430.
30 J. Cai, R. Javed, D. Ye, H. Zhao and J. Zhang, *J. Mater. Chem. A*, 2020, **8**, 22467–22487.
31 J. Sivakumar, C. Premkumar, P. Santhanam and N. Saraswathi, *Afr. J. Basic Appl. Sci.*, 2011, **6**, 265–270.
32 M. S. Hudlikar, M. Joglekar, M. Dhaygude and K. Kodam, *J. Nanopart. Res.*, 2020, **5**, 1–6.
33 Z. L. Wang, *Adv. Mater.*, 2000, **17**, 1295–1298.
34 M. B. Gawande, A. Goswami, F.-X. Felpin, T. Asefa, X. Huang, R. Silva, X. Zou, R. Zboril and R. S. Verma, *Chem. Rev.*, 2016, **6**, 3722–3811.
35 L. Yu-Syuan, Y.-F. Lin, A. Nain and Y.-F. Huang, *Sens. Actuators Rep.*, 2021, **3**, 100026.
36 Y. Xue, Z. Cheng, M. Luo, H. Hu and C. Xia, *Biosensors*, 2021, **11**, 424.
37 M. I. Din and R. Rehan, *Anal. Lett.*, 2016, **1**, 50–62.
38 R. Jin, *Nanoscale*, 2015, **7**, 1549–1565.
39 S. Dehnen, A. Eichhöfer and D. Fenske, *Eur. J. Inorg. Chem.*, 2002, **2002**, 279.
40 O. Fuhr, S. Dehnen and D. Fenske, *Chem. Soc. Rev.*, 2013, **42**, 1871–1906.
41 C. Coughlan, M. Ibáñez, O. Dobrozhan, A. Singh, A. Cabot and K. M. Ryan, *Chem. Rev.*, 2017, **117**, 5865–6109.
42 A. Baghdasaryan and T. Bürgi, *Nanoscale*, 2021, **13**, 6283–6340.
43 K. K. Aswini, A. M. Vinu Mohan and V. M. Biju, *Mater. Sci. Eng., C*, 2014, **37**, 321–326.
44 H.-S. Hashemi, A. Nezamzadeh-Ejhieh and M. Karimi-Shamsabadi, *Mater. Sci. Eng., C*, 2016, **58**, 286–293.
45 S. Wu, X. Lan, F. Huang, Z. Luo, H. Ju, C. Meng and C. Duan, *Biosens. Bioelectron.*, 2012, **32**, 293–296.
46 K. R. Atkuri, J. J. Mantovani, L. A Herzenberg and L. A. Herzenberg, *Curr. Opin. Pharmacol.*, 2007, **7**, 355–359.

47 P. Mulpur, A. Kurdekar, R. Podila, A. M. Rao and V. Kamisetti, *Nanotechnol. Rev.*, 2015, **4**, 1–18.
48 N. Cebi, C. E. Dogan, A. Develioglu, M. E. A. Yayla and O. Sagdic, *Food Chem.*, 2017, **1**, 116–124.
49 C. E. Dogan, N. Cebi, A. Develioglu, E. O. Olgun and O. Sagdic, *J. Cereal Sci.*, 2018, **84**, 49–54.
50 K. V. Harisha, B. E. Kumara Swamy, P. S. Ganesh and H. Jayadevappa, *J. Electroanal. Chem.*, 2019, **832**, 486–492.
51 J. Zhou, Y. Chen, L. Lan, C. Zhang, M. Pan, Y. Wang, B. Han, Z. Wang, J. Jiao and Q. Chen, *Anal. Bioanal. Chem.*, 2019, **567**, 51–62.
52 W. Khamcharoen, C. S. Henry and W. Siangproh, *Talanta*, 2022, **237**, 122983.
53 J. Faintuch, P. B. Aguilar and W. Nadalin, *Nutrition*, 1999, **15**, 177–179.
54 S. M. Zhang, W. C. Willett, J. Selhub, J. E. Manson, G. A. Colditz and S. E. Hankinson, *Cancer Epidemiol., Biomarkers Prev.*, 2003, **12**, 1188–1193.
55 K. Saito, *Biochem. Biotechnol.*, 1999, 267–291.
56 R. L. Krauthsiegel, L. Baratova and R. H. Schirmer, *Angew. Chem., Int. Ed.*, 2005, **44**, 690–715.
57 X. Dai, Q. H. Wu, P. C. Wang, J. Tian, Y. Xu, S. Q. Wang, J. Y. Miao and B. X. Zhao, *Biosens. Bioelectron.*, 2014, **59**, 35–39.
58 L. Duan, Y. Xu, X. Qian, F. Wang, J. Liu and T. Cheng, *Tetrahedron Lett.*, 2008, **49**, 6624–6627.
59 O. Rusin, N. N. S. Luce, R. A. Agbaria, J. O. Escobedo, S. Jiang, I. M. Warner, F. B. Dawan, K. Lian and R. M. Strongin, *J. Am. Chem. Soc.*, 2004, **126**, 438–439.
60 W. Wang, O. Rusin, X. Xu, K. K. Kim, J. O. Escobedo, S. O. Fakayode, K. A. Fletcher, M. Lowry, C. M. Schowalter and C. M. Lawrence, *J. Am. Chem. Soc.*, 2005, **127**, 15949–15958.
61 B. Sharma and M. K. Rabinal, *J. Alloys Compd.*, 2015, (649), 11–18.
62 R. J. Spears, C. McMohan and V. Chudasama, *Chem. Soc. Rev.*, 2021, **50**, 11098–11155.
63 S. Mandal, A. Gole, N. Lala, R. Gonnade, V. Ganvir and M. Sastry, *Langmuir*, 2001, **17**, 6262–6268.
64 M. Martínez-Carmona, C. Cela, V. A. Kuznetsova, J. A. Geoghegan and Y. K. Gun'ko, *J. Mater. Chem. B*, 2021, **9**, 3544–3553.
65 S. Devi, R. K. Gupta, A. K. Paul and S. Tyagi, *Mater. Res. Express*, 2019, **6**, 025605.
66 S. Chauhan and L. S. B. Upadhyay, *MethodsX*, 2018, **5**, 1528–1533.
67 A. R. Ivanov, I. V. Nazimov and L. A. Baratova, *J. Chromatogr. A*, 2000, **87**, 433–442.
68 A. R. Ivanov, I. V. Nazimov and L. Baratova, *J. Chromatogr. A*, 2000, **895**, 157–166.
69 G. Chen, L. Zhang and J. Wang, *Talanta*, 2004, **64**, 1018–1023.
70 T. Inoue and J. R. Kirchhoff, *Anal. Chem.*, 2000, **72**, 5755–5760.
71 M. Wen, H. Liu, F. Zhang, Y. Zhu, D. Liu, T. Yang and Q. Wu, *Chem. Commun.*, 2009, **30**, 4530–4532.
72 J. Zhu, A. Ilirian Dhimitruka and D. Pei, *Org. Lett.*, 2004, **6**, 3809–3812.
73 S. Fei, J. Chen, S. Yao, G. Deng, D. He and Y. Kuang, *Anal. Biochem.*, 2005, **339**, 29–35.
74 M. Rafii, R. Elango, G. Courtney-Martin, J. D. House, L. Fisher and P. B. Pencharz, *Anal. Biochem.*, 2007, **371**, 71–81.
75 M. Zhang, M. Yu, F. Li, M. Zhu, M. Li, Y. Gao, L. Li, Z. Liu, J. Zhang and D. Zhang, *J. Am. Chem. Soc.*, 2007, **129**, 10322–10323.
76 S. Hajizadeh, K. Farhadi, M. Forough and R. Molaei, *Anal. Methods*, 2012, **4**, 1747–1752.
77 J. S. Lee, P. A. Ulmann, M. S. Han and C. A. Mirkin, *Nano Lett.*, 2008, **8**, 529–533.
78 H. Li, J. Fan, J. Wang, M. Tian, J. Du, S. Sun, P. Sun and X. Peng, *Chem. Commun.*, 2009, **45**, 5904–5906.
79 H. M. Liu, G. Mei, S. Chen and Y. F. Long, *Anal. Methods*, 2017, **9**, 3249–3254.
80 M. Ganguly, A. Pal, Y. Negishi and T. Pal, *Langmuir*, 2013, **29**, 2033–2043.
81 M. Ganguly, J. Jana, A. Pal and T. Pal, *RSC Adv.*, 2016, **6**, 17683–17703.
82 K. M. Dokken, J. G. Parsons, J. McClure and J. L. Gardea-Torresdey, *Inorg. Chim. Acta*, 2009, **362**, 395–401.
83 V. M. Rao, D. N. Sathyanarayana and H. Manohar, *J. Chem. Soc., Dalton*, 1983, **10**, 2167.
84 R. L. Lieberman, D. B. Shrestha, P. E. Doan, B. M. Hoffman, T. L. Stemmler and A. C. Rosenzweig, *Proc. Natl. Acad. Sci. U. S. A.*, 2003, **100**, 3820.
85 L. Pecci, G. Montefoschi, G. Musci and D. Cavallini, *Amino Acids*, 1997, **13**, 355–367.
86 B. K. Maiti, L. B. Maia, A. J. Moro, J. C. Lima, C. M. Cordas, I. Moura and J. J. G. Moura, *Inorg. Chem.*, 2018, **14**, 8078–8088.
87 A. Rigo, A. Corazza, M. L. D. Paolo, M. Rossetto, R. Ugolini and M. Scarpa, *J. Inorg. Biochem.*, 2004, **9**, 1495–1501.
88 K. B. A. Ahmed, M. Sengan, S. P. Kumar and A. Veerappan, *Sens. Actuators, B*, 2016, **233**, 431–437.
89 X. Xu, N. Zhang, G. M. Brown, T. G. Thundat and H.-F. Ji, *Appl. Biochem. Biotechnol.*, 2017, **2**, 555–565.
90 L. Tang, L. Zhu, F. Tang, C. Yao, J. Wang and L. Li, *Langmuir*, 2018, **48**, 14570–14576.
91 M. C. Pan, Y. M. Lei, Y. Q. Chai, R. Yuan and Y. Zhou, *Anal. Chem.*, 2020, **19**, 13581–13587.
92 L. Yuan, M. Liang, M. Hummel, C. Shao and S. Lu, *Chemosensors*, 2023, **11**, 159.
93 Y. D. Choi, N. H. Ho and C. H. Tung, *Angew. Chem.*, 2007, **46**, 707–709.
94 R. Z. Ouyang, W. Y. Zhang, S. L. Zhou, Z. L. Xue, L. N. Xu, Y. Y. Gu and Y. Q. Miao,I, *Electrochim. Acta*, 2013, **11**, 686–693.
95 C. K. B alavigneswaran, T. S. J. Kumar, R. M. Packiaraj and S. Prakash, *Appl. Nanosci.*, 2014, **4**, 367–378.
96 S. Vallejos, A. Muñoz, F. C. García, F. Serna, S. Ibeas and J. M. García, *J. Hazard. Mater.*, 2012, **227**, 480–483.
97 X. D. Yang, Y. N. Jiang, B. W. Shen, Y. Chen, F. X. Dong, K. Yu, B. Yang and Q. Lin, *Polym. Chem.*, 2013, **4**, 5591–5596.

98 K. A. N. Upamali, L. A. Estrada and D. C. Neckers, *Anal. Methods*, 2011, **3**, 2469–2471.
99 M. Cui, G. Song, C. Wang and Q. Song, *Microchim. Acta*, 2015, **182**, 1371–1377.
100 M. Zhang, G. Liu, K. Song, Z. Wang, Q. Zhao, S. Li and Z. Ye, *Chem. Eng. J.*, 2015, **259**, 876–884.
101 S. Yang, X. Sun and Y. Chen, *Adv. Mater. Lett.*, 2017, **194**, 5–8.
102 R. Mu, H. Shi, Y. Yuan, A. Karnjanapiboonwong and M. Burken, *Anal. Chem.*, 2012, **84**, 3427–3432.
103 S. Babaee and A. Beiraghi, *Anal. Chim. Acta*, 2010, **662**, 9–13.
104 V. Bhalla, A. Gupta, M. Kumar, D. S. Rao and S. K. Prasad, *ACS Appl. Mater. Interfaces*, 2013, **5**, 672–679.
105 G. Hambarde, S. Bothra, Y. Upadhyay, R. K. Bera and S. K. Sahoo, *Microchem. J.*, 2019, **147**, 899–904.
106 K. Shanmugaraj and S. Abraham John, *New J. Chem.*, 2018, **42**, 7223–7229.
107 P. Srinivasan, M. Gunasekaran, T. Kanagasekaran, R. Gopalakrishnan and P. Ramasamy, *J. Cryst. Growth*, 2006, **289**, 639–646.
108 S. Kumar, N. Venkatramaiah and S. Patil, *J. Phys. Chem.*, 2013, **117**, 7236–7245.
109 S. Shanmugaraju, S. A. Joshi and P. S. Mukherjee, *J. Mater. Chem.*, 2011, **21**, 9130–9138.
110 Y. Ma, H. Li, S. Peng and L. Wang, *Anal. Chem.*, 2012, **84**, 8415–8421.
111 A. Chowdhury and P. S. Mukherjee, *J. Org. Chem.*, 2015, **80**, 4064–4075.
112 S. S. Nagarkar, A. V. Desai, P. Samanta and S. K. Ghosh, *Dalton Trans.*, 2015, **44**, 15175–15180.
113 J. Akhavan, *Chemistry of Explosives*, Royal Society of Chemistry, 2nd edn, 2004*Innovative Treatment Technologies: Annual Status Report*, U. S. Environmental Protection Agency, Washington, D. C., 8th edn, 1996.
114 S. Hussain, A. H. Malik, M. A. Afroz and P. K. Iyer, *Chem. Commun.*, 2015, **51**, 7207–7210.
115 S. K. Patil, D. V. Awale, M. M. Vadiyar, S. A. Patil, S. C. Bhise, A. H. Gore, G. B. Kolekar, J. H. Kim and S. S. Kolekar, *ChemistrySelect*, 2017, **2**, 4124–4130.
116 S. S. Nagarkar, A. V. Desai and S. K. Ghosh, *CrystEngComm*, 2016, **18**, 2994–3007.
117 S. Chen, Y. L. Yu and J. H. Wang, *Anal. Chim. Acta*, 2018, **999**, 13–26.
118 Y.-S. Borghei, M. Hosseini, M. Khoobi and M. R. Ganjali, *J. Fluoresc.*, 2016, **27**, 529–536.
119 D. Badocco, P. Pastore, G. Favaro and C. Macca, *Talanta*, 2007, **72**, 249.
120 W. Ruengsitagoon, S. Liawruangrath and A. Townshend, *Talanta*, 2006, **69**, 976.
121 X. Wang, H. C. Zhao, L. H. Nie, L. P. Jin and Z. L. Zhang, *Anal. Chim. Acta*, 2001, **445**, 169.
122 W. B. Liu and Y. M. Huang, *Anal. Chim. Acta*, 2004, **506**, 183.
123 T. Wiggins, S. Kumar, S. R. Markar, S. Antonowicz and G. B. Hanna, *Cancer Epidemiol., Biomarkers Prev.*, 2015, **24**, 33.
124 J. M. Silván, J. van de Lagemaat, A. Olano and M. D. del Castillo, *J. Pharm. Biomed. Anal.*, 2006, **41**, 1543.
125 U. Lichter-Konecki, C. Hipke and D. Konecki, *Mol. Genet. Metab.*, 1999, **316**, 308.
126 Y. S. Borghei, M. Hosseini, M. Khoobi and M. R. Ganjali, *Luminescence*, 2017, **32**, 1045–1050.
127 C. Zhang, M. Liang, C. Shao, Z. Li, X. Cao, Y. Wang, Y. Wu and S. Lu, *ACS Appl. Bio Mater.*, 2023, **3**, 1283–1293.
128 Q. Shi, J. Huang, Y. Sun, R. Deng, M. Teng, Q. Li, Y. Y. Yang, X. F. Hu, Z. J. Zhang and G. Zhang, *Mikrochim. Acta*, 2018, **185**, 1–8.
129 Z. Zhang and H. Cheng, *Crit. Rev. Anal. Chem.*, 2017, **47**, 223–250.
130 N. Lian, Y. Zhang, J. Tang and H. Wu, *Microchem. J.*, 2021, **164**, 105989.
131 V. Uivarosi, *Molecules*, 2013, **18**, 11153–11197.
132 P. Novotna, F. Kralik and M. Urbanova, *Biophys. Chem.*, 2015, **205**, 41–50.
133 M. Martelanc, L. Ziberna, S. Passamonti and M. Franko, *Talanta*, 2016, **154**, 92–98.
134 R. S. Aparna, J. S. Anjali devi, N. John, K. Abha, S. S. Syamchand and S. George, *Spectrochim. Acta, Part A*, 2018, **199**, 123–129.
135 S. K. Anand, M. R. Mathew and K. G. Kumar, *J. Fluoresc.*, 2019, **30**, 63–70.
136 P. Jolles, *Exper. Suppl.*, 1996, **75**, 449.
137 R. Swaminathan, V. K. Ravi, S. Kumar, M. V. S. Kumar and N. Chandra, *Adv. Protein Chem. Struct. Biol.*, 2011, **84**, 63–111.
138 L. Callewaert and C. W. Michiels, *J. Biosci.*, 2010, **35**, 127–160.
139 L. Yan, S. Shen, J. Yun and K. Yao, *Chin. J. Chem. Eng.*, 2011, **19**, 876–880.
140 S. S. Levinson, R. J. Elin and L. Yam, *Clin. Chem.*, 2002, **48**, 1131–1132.
141 M. Sonaimuthu, Y. Nerthigan, N. Swaminathan, N. Sharma and H. F. Wu, *Anal. Bioanal. Chem.*, 2020, **412**, 7141–7154.
142 I. Eli, *Laussnne – Printed in the Netherlands*, 1981, pp. 85–101.
143 D. Mott, J. Galkowski, L. Wang, J. Luo and C. J. Zhong, *Langmuir*, 2007, **23**, 5740–5745.
144 K. P. Hakala, P. M. Tuomainen, M. J. Yli-Halla and H. Hartikainen, *J. Environ. Sci. Health, Part B*, 2014, **49**, 491–497.
145 X. Feng, K. Wang, Z. Mu, Y. Zhao and H. Zhang, *Am. J. Potato Res.*, 2015, **292**, 567–572.
146 L. Li, C. Hou, J. Li, Y. Yang, J. Hou, Y. Ma, Q. He, H. Luo and D. Huo, *Anal. Methods*, 2019, **11**, 4637–4643.
147 S. C. Howard, J. McCormick, C.-H. Pui, R. K. Buddington and R. D. Harvey, *Oncologist*, 2016, **12**, 1471–1482.
148 H. L. Van, A. A. M. Heemskerk, M. L. Becker, J. S. Leeder and J. F. Stobaugh, *Anal. Methods*, 2010, **2**, 831.
149 D. Asbahr, L. C. S. Figueiredo-Filho, F. C. Vicentini, G. G. Oliveira, O. Fatibello-Filho and C. E. Banks, *Sens. Actuators, B*, 2013, **188**, 334–339.
150 X. Yuan, X. Dou, K. Zheng and J. Xie, *Part. Part. Syst. Charact.*, 2015, **32**, 613–629.
151 Y. Nerthigan, A. K. Sharma, S. Pandey and H.-F. Wu, *Microchim. Acta*, 2019, **186**, 3.

152 A. P. de Silva, D. B. Fox, A. J. M. Huxley and T. S. Moody, *Coord. Chem. Rev.*, 2000, **205**, 41–57.
153 F. A. Cotton, C. A. Murillo, M. Bochmann, *Advanced inorganic chemistry*, John Wiley & Sons, New York, 6th edn, 1999.
154 P. B. Tchounwou, W. K. Ayensu, N. Ninashvili and D. Sutton, *Environ. Toxicol.*, 2003, **18**, 149–175.
155 T. W. Clarkson, L. Magos and G. J. Myers, *N. Engl. J. Med.*, 2003, **349**, 1731–1737.
156 Y. Wang, F. Yang and X. Yang, *Biosens. Bioelectron.*, 2010, **25**, 1994–1998.
157 R. A. Soomro, A. Nafady Sirrajudin, N. Memon, T. H. Sherazi and N. H. Kalwar, *Talanta*, 2014, **130**, 414–422.
158 Y. Ma, H. Mei, Y. Li, P. Zhou, G. Mao, H. Wang and X. Wang, *Food Chem.*, 2022, **379**, 132155.
159 R. Rajamanikandan and M. Ilanchelian, *Sens. Actuators, B*, 2017, **244**, 380–386.
160 R. Rajamanikandana, B. Aazaadb, S. K. Lakshmipathib and M. Ilanchelian, *Microchem. J.*, 2020, **158**, 105253.
161 C. Wang and Y. Huang, *Nano*, 2013, **8**, 1350054–1350063.
162 Y. Zhang, Z. Shao, W. Yuan, H. Xu, X. You and X. Liao, *Materialia*, 2021, **20**, 101232.
163 S. Panigrahi, S. Kundu, S. Basu, S. Praharaj, S. Jana, S. Pande, S. K. Ghosh, A. Pal and T. Pal, *J. Phys. Chem. C*, 2007, **4**, 1612–1619.
164 S. Priscilla, D. Sivaramakrishna and V. Anbazhagan, *Thermochim. Acta*, 2014, **586**, 25.
165 Y. Xu, S. Szep and Z. Lu, *Proc. Natl. Acad. Sci. U. S. A.*, 2009, **106**, 20515–20519.
166 J. Zhang, X. Xu, Y. Yuan, C. Yang and X. Yang, *ACS Appl. Mater. Interfaces*, 2011, **3**, 2928–2931.